Effect of Carbon Concentration on Changing the Morphology of Titanium Carbide Nanoparticles from Cubic to Cuboctahedron

David E. Grove, Ujjwal Gupta, and A. W. Castleman, Jr.*

Departments of Chemistry and Physics, The Pennsylvania State University, University Park, Pennsylvania 16802

ABSTRACT Titanium carbide nanoparticles were synthesized by flowing methane through a plasma generated from an arc discharge between two titanium electrodes. Different methane concentrations were employed in studies made to investigate the effects of carbon concentration on particle morphology. Transmission electron microscopy and X-ray diffraction were used to investigate the synthesized TiC nanopowders, whereupon it was found that nanocrystalline TiC nanoparticles prefer a cubic morphology at low concentrations of methane and a cuboctahedron morphology at high concentration of methane. The change in particle morphology is attributed to carbon affecting the relative growth rates of the {111} and {100} facets on a TiC seed crystal.

KEYWORDS: titanium carbide · arc discharge · carbide catalysis · nanoparticle morphology control

Early transition metal carbides are well-known for their high melting points, high degree of hardness, and thermal and electrical conductivity.[1−6] These properties make early transition metal carbides very useful in coatings, tools, machine parts, and as reinforcements in composites.[1−6] They often adopt simple crystal structures, such as face-centered cubic (fcc), body-centered cubic (bcc), or simple hexagonal (hex) structure, with the nonmetal elements occupying the interstitial spaces between metal atoms.[7] Theoretical band-structure calculations indicate that the bonding in carbides involves simultaneous contributions from metallic, covalent, and ionic bonding.[8−11] Metallic bonding is related to the metal−metal bonds; covalent bonding arises from the interaction of carbon 2s and 2p orbitals with metal d orbitals; and the ionic contribution is related to the charge transfer between metal and carbon atoms.

The properties of a nanoparticle are determined by a set of physical parameters that include its size, shape, composition, and structure. In the case of catalysis, it is well-established that for certain systems the activity of a nanoparticle can be enhanced by reducing its size, thereby increasing the surface area and the availability of defects.[12−15] Transition metal carbides have attracted considerable attention for catalytic applications since 1973, when Levy and Boudart first reported the Pt-like behavior of WC in the neopentane isomerization reaction.[16] Some clear advantages that early transition metal carbides have over their parent metal include activity, selectivity, and durability.[17,18] The selectivity is most sensitive to the packing of atoms on the surface or exposed facets of a nanoparticle.[19,20] Different crystal surfaces exhibit different physical and chemical properties due to their packing and coordination state. For example the {111}, {100}, and {110} surfaces of a face-centered cubic (fcc) metal have different surface atom densities, electronic structures, and chemical reactivities. The TiC {111} surface has been shown to be highly active for dissociative adsorption of hydrogen at room temperature.[21] The TiC {100} surface has shown the ability to adsorb several different molecules including water, methanol, ethanol, 2-propanol, NH_3, CO, and methyl formate.[22−26] Also adsorption and dissociation of O_2 and SO_2 has been studied on the TiC {001} surface.[27−32]

Traditionally, titanium carbide (TiC) has been synthesized as either thin films or micrometer-sized particles. TiC thin films can be deposited through the reaction of $TiCl_4$ with gaseous hydrocarbons or magnesium reduction of $TiCl_4$ and CCl_4.[33] Early transition metal carbide micrometer-sized particles are commercially made by carbothermal reduction of metal oxide.[34] The shape and size of the metal carbides particle depends on the shape and size of the

*Address correspondence to awc@psu.edu.

Received for review August 19, 2009 and accepted December 3, 2009.

Published online December 15, 2009.
10.1021/nn9010413

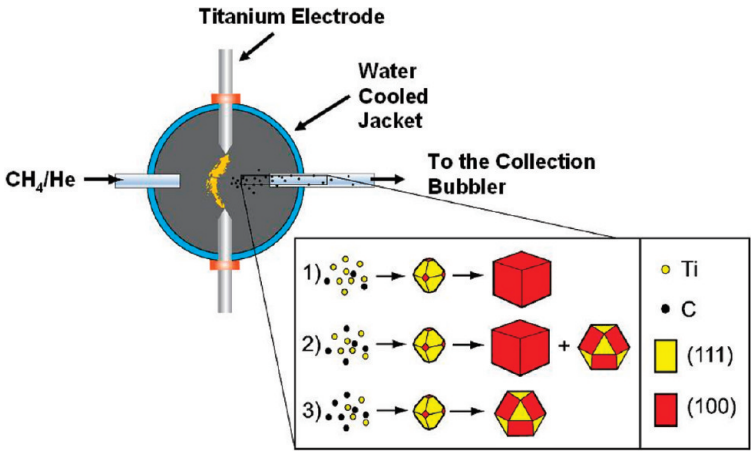

Figure 1. Principle components of the arc discharge vessel and the different nanoparticle morphologies with varying carbon concentrations. The black spheres represent carbon atoms, and the yellow spheres represent titanium atoms.

starting metal oxide particle. Titanium carbide nanopowders have been formed through thermal plasma processing with an average size of less than 100 nm.[5] The preparation of nanoparticles with different shapes and surface facets is therefore important for controlling their properties. The role of carbon concentration on how it affects titanium carbide nanoparticle morphology will be presented and discussed.

RESULTS AND DISCUSSION

Titanium carbide nanoparticles were synthesized by an arc discharge method with varying methane concentrations, as summarized in Figure 1. A typical XRD pattern of the synthesized ultrafine, black powder collected in the bubbler is shown in Figure 2, clearly confirming the presence of titanium carbide (TiC) without any evidence of impurities such as titanium dioxide or pure titanium metal. The peaks in the XRD pattern are broad due to the scattering effects from the small particle size of the powders.[35,36] Particle size can be calculated from XRD patterns by using the Scherrer equation:

$$\text{particle size} = K\lambda/d\cos\theta \qquad (1)$$

where λ is the wavelength of the X-ray radiation source, d is the full width half-maximum (fwhm) of the peak, θ is the Bragg angle, and K is a constant with a typical value of 0.9.[37] It is desirable to use peaks at smaller diffraction angles to reduce the effect of lattice strain.[38] From the peak of $2\theta = 35.55$ in Figure 2, particle size is calculated using the Scherrer equation to be 20 nm for nanoparticles produced with 12% methane concentration, which is in good agreement with TEM images from the sample.

Particles formed from gas mixtures of 5% and 12% methane are shown in the TEM images in Figure 3 panels a and b, respectively. The images also show that the particles formed are uniform cubes with no excess amorphous carbon. The varying contrast from nanoparticle to nanoparticle is due to different orientations of the particles in the electron beam. Single particle diffraction patterns show that the nanoparticles are single crystals with all six facets on the cube being {100}. A selected area diffraction pattern shown in Figure 3c has d-spacings that measure 2.50, 2.16, and 1.53 that match with bulk titanium carbide with fcc structure. Figure 3d is a typical EDS spectrum of the synthesized nanoparticles showing peaks corresponding to titanium and carbon from the nanoparticles. The lacey carbon-coated grids also contribute to the carbon signal. The copper peaks in the EDS spectra are from the lacey carbon-coated copper TEM grids on which the particles are deposited. Another interesting observation is that there is no visible oxygen peak in the EDS spectra.

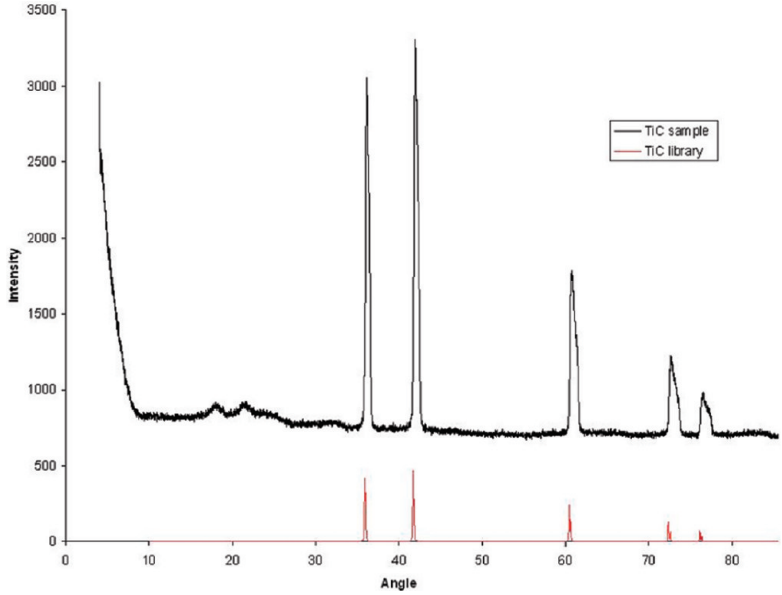

Figure 2. XRD pattern of titanium carbide nanopowders compared to a library spectrum for bulk titanium carbide.

A TEM image of TiC nanoparticles synthesized under a gas mixture of 30% methane is shown in Figure 4a. The image shows a transformation from cube-dominated morphology to a mixture of cubes and cuboctahedron-shaped particles. Selected area diffraction patterns show that both particle morphologies are TiC with fcc structure. Also single particle diffraction patterns show that both morphologies are single crystals.

Figure 4b,c shows the TEM images of nanoparticles formed with 60% and 100% methane, respectively. The morphology of the nanoparticles is now dominated by the cuboctahedron-shaped nanoparticles. This gives each of the nanoparticles 14 facets

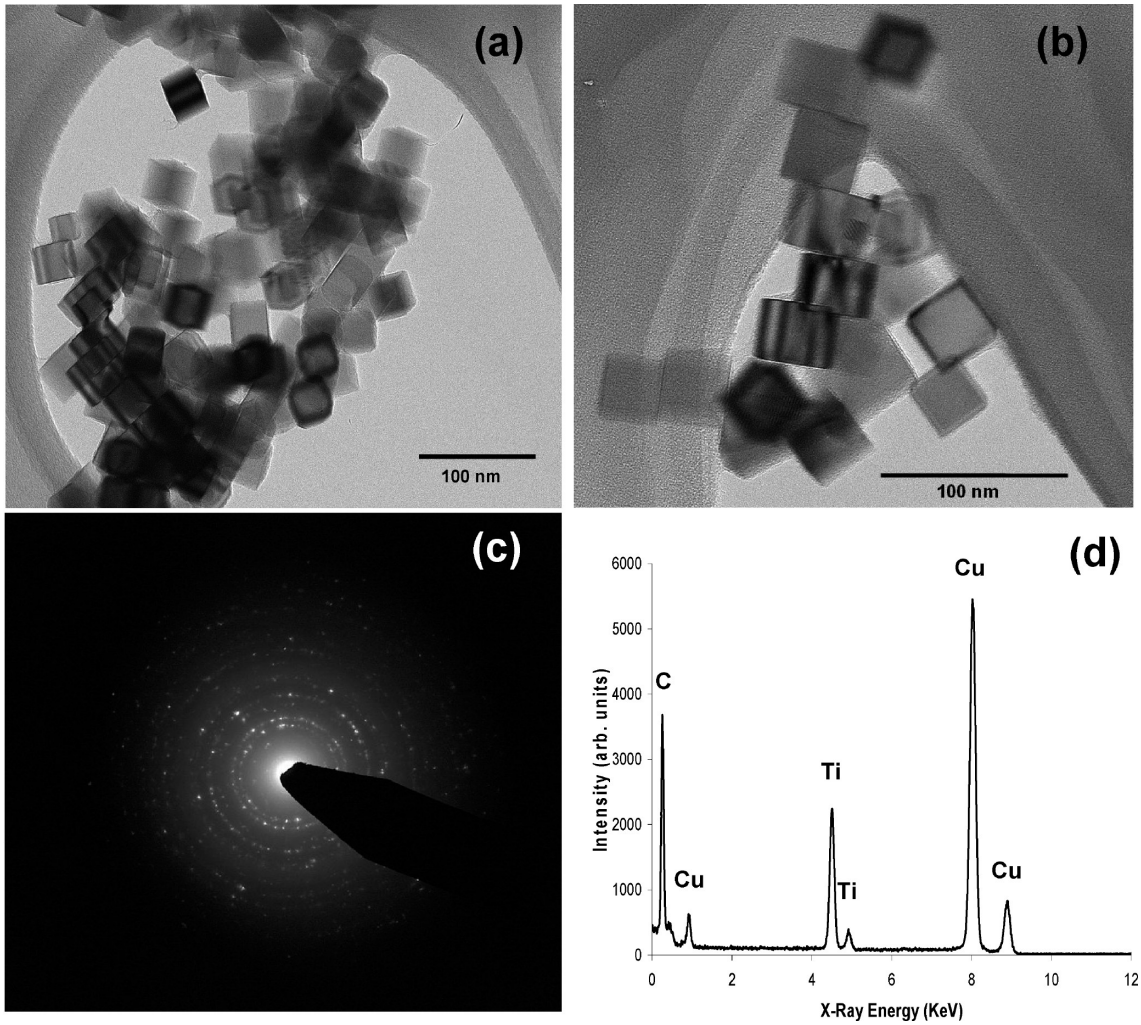

Figure 3. (a−b) TEM images of cube-shaped nanoparticles synthesized with 5% and 12% methane. (c) A selected area diffraction of the synthesized titanium carbide nanoparticles confirms the nanoparticles are titanium carbide. The three inner rings have a *d*-spacing measurement of 2.50, 2.16, and 1.53. (d) EDS spectra of the synthesized titanium nanoparticles showing only titanium, carbon, and copper present. The copper and a portion of the carbon signal is from the TEM grid.

that have a combination of 6 {100} and 8 {111} facets. Selected area diffraction patterns confirm that the nanoparticles are TiC with an fcc crystal structure. Some of the nanoparticles synthesized with 100% methane show an amorphous carbon shell around the nanoparticles. The ability to affect morphology changes from cubic to cuboctahedron with increasing methane concentration is reproducible as verified in a number of experiments.

We measured the shape distribution of the titanium nanoparticles from multiple TEM images from various methane concentrations in Figure 4d. For each methane concentration we counted between 100 and 160 nanoparticles. (Only clearly visible nanoparticles were counted and large agglomerations where the morphology of the nanoparticles was not clear were excluded. The large agglomerations made up less than 10% of the sample and did not affect the morphology trend.)

Nanoparticles synthesized with 5% and 12% methane concentrations contained 94% and 86% cubes, respectively. With 30% methane the nanoparticles are split with 58% being cubes and 42% being cuboctahedrons. The cuboctahedron morphology dominates with 60% and 100% methane where 93% and 94% of the samples are cuboctahedrons.

To understand this phenomenon of changes in morphology with carbon concentration we looked into the relationship of surface energy with the growth rate of the different facets. As clusters grow past a critical size they form seed crystals which have well-defined crystallographic facets.[39] Under thermodynamic control the seed crystal should take on a morphology that minimizes the exposed surface and maximizes the volume. Typically the most stable morphology follows Wulff's theorem,[40] which attempts to minimize the total interfacial free energy of a system within a given volume. For an fcc structure material the surface energy (γ) for the different facets follows an energy sequence of $\gamma_{\{111\}} < \gamma_{\{100\}} < \gamma_{\{110\}}$.[39] Therefore a single crystal seed should take on the shape of an octahedral in order to maximize the number of {111} facets and minimize the sur-

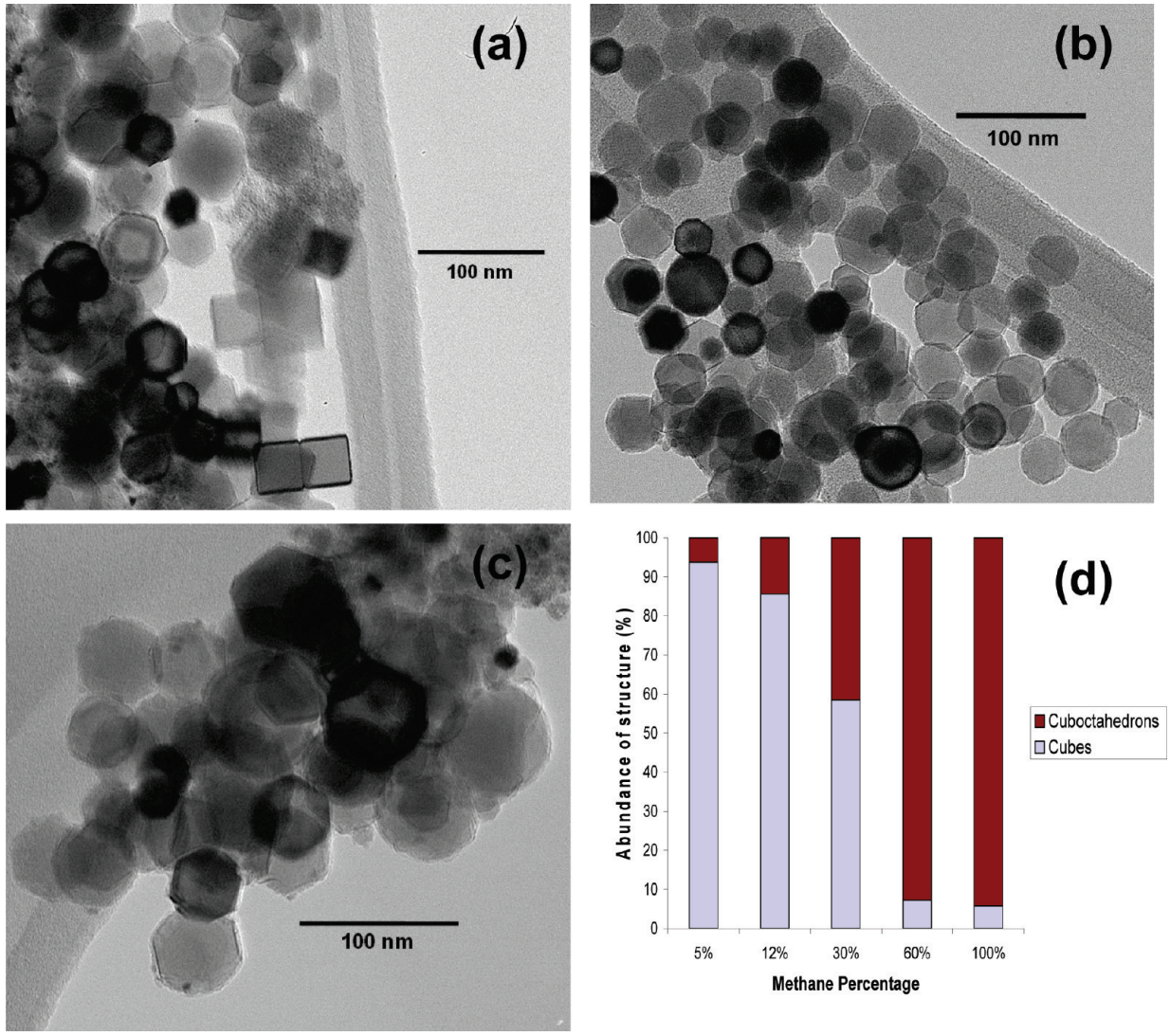

Figure 4. (a−c) TEM images of titanium carbide nanoparticles synthesized with 30% (a), 60% (b), and 100% methane. Panel d is a bar graph displaying the abundance of different morphologies synthesized with varying methane concentrations. Cubes dominate at low methane concentrations and cuboctahedrons dominate at high methane concentrations.

face energy.[39] However, this shape has a large surface area compared to its volume resulting in the high energy vertices to be truncated. The seed crystals therefore form into the shape of a truncated octahedron enclosed by a combination of {111} and {100} facets.[39]

Referring back to the results, we notice that at lower concentrations of methane, cubic morphology is dominant and at higher concentrations, cuboctahedrons are dominant. However, irrespective of the carbon concentration, the TiC nanoparticles have 1:1 stoichiometry which rules out the morphology change being due to different stoichiometries. Now, according to periodic bond chain (PBC) theory nomenclature, {100} faces are flat surfaces and are called F-faces.[41,42] The {111} faces are kinked surfaces and are called K-faces. Each surface site on the K-faces is a kink site and irreversibly incorporates incoming atoms absorbed on the surface. K-faces therefore produce a surface that has many nucleation sites causing a higher growth rate. However impurities and solvent molecules have been shown to interact with the K-faces, thereby decreasing the growth rate of these facets.[43,44] In our case the excess carbon interacts with the kink sites on the K-faces. The TiC nanoparticles synthesized with 5% and 12% methane concentrations produce nanoparticles that are cubic having six {100} facets. This can be explained within the PBC theory model. The seed crystal is a truncated octahedron which has a mix of {100} and {111} facets. Since at low supersaturation levels (corresponding to 5% and 12% methane), the growth rate for ⟨111⟩ is faster than the ⟨100⟩ direction, they finally end up forming cubic nanoparticles possessing all six {100} facets, as depicted in Figure 1. At higher carbon concentration (60%, 100%) the TiC nanoparticles are cuboctahedron shaped. The decrease in the growth rate of the {111} facet is because of the interactions between excess carbon and the kink sites. The excess carbon leads both ⟨100⟩ and ⟨111⟩ facets to have similar growth rates and the seed crys-

tal truncated octahedron shape becomes only slightly distorted to the cuboctahedron shape.

At 30% methane concentration both processes are playing a part and therefore a mixture of cubic and cuboctahedron particles are observed. This might also be influenced by a localized concentration/pressure gradient produced during the atomization process. The inner region of the metal and carbon vapor promotes the cuboctahedron-shaped particles, while in the outer region where the metal and carbon atoms are in lower concentration, the formation of cubes dominates.

CONCLUSIONS

We have shown that titanium carbide nanoparticles can be synthesized through an arc discharge method. The nanoparticle morphology can be controlled by changing methane concentration. TiC cubes are synthesized at a low methane concentration and cuboctahedrons at a high methane concentration. Both the cubes and the cuboctahedrons are formed from a truncated octahedron seed crystal and have fcc structure. However, the difference in morphology arises because of the difference in the growth rates between {111} facet and the {100} facet at different carbon levels. To the best of our knowledge this is the first study to show control over nanoparticle morphology for early transition metal carbides. There is no capping agent used to stabilize the titanium nanoparticle surface, therefore the bare nanoparticles could potentially be important for applications in the fields of catalysis and ceramic processing. Several experimental studies are in progress where the effect of current, flow rate, and time are being controlled to observe an effect on morphology of the TiC nanoparticles. It will also be interesting to study how the size of particles is affected by changing each of these conditions.

METHODS

Materials. Pure metal Ti (purity 99.7%) rods (6.4 mm in diameter) were purchased from Alfa Aesar. Methane (purity 99%) and helium (purity 99.999%) were purchased from BOC Gases and Praxair, respectively. The arc discharge vessel was homemade and the power supply for the arc discharge was a Caftsman 240AC/180DC arc welder.

Nanoparticle Synthesis. Various combinations of methane in helium ranging from 5% to 100% methane were used as reactant gas mixtures. The gas mixture flow rate was maintained at 40 standard cubic centimeters per minute (sccm) and a discharge was acquired by applying 180A direct current for a period of 10 min. Titanium and methane were atomized within the arc discharge generated plasma. Once the metal and carbon vapor is sufficiently cooled or the concentration is high enough nucleation occurs and is followed by nanoparticle growth. The titanium carbide nanoparticles were entrained in the helium gas flow and were collected from the helium flow in a bubbler containing acetonitrile.

Characterization. The synthesized nanoparticles were characterized by powder X-ray diffraction (XRD) using Cu Kα radiation (λ = 1.5405 Å). A couple of drops of solution were place on a 200 mesh lacey carbon-coated copper grids for TEM analysis. The morphology, size, and composition of the nanoparticles were characterized using Philips EM-420T transmission electron microscopy operating at an accelerating voltage of 120 kV equipped with energy dispersive spectroscopy (EDS) and selected area diffraction patterns (SADP) capabilities.

Acknowledgment. The authors acknowledge support by the AFOSR Grant No. FA-9550-07-1-0151. We thank Professor Jim Adair for his helpful discussions and suggestions. We also thank the Materials Research Institute TEM facility at The Penn State University, University Park. We also thank Kristin Cederquist for her help in making the instrumentation figure.

REFERENCES AND NOTES

1. Li, Y.-L.; Takamasa, I. Incongruent Vaporization of Titanium Carbide in Thermal Plasma. *Mater. Sci. Eng., A* **2003**, *345*, 301–308.
2. Lee, D. W.; Alexandrovskii, S. V.; Kim, B. K. Novel Synthesis of Substoichiometric Ultrafine Titanium Carbide. *Mater. Lett.* **2004**, *58*, 1471–1474.
3. Gotoh, Y.; Fujimura, K.; Koike, M.; Ohkoshi, Y.; Nagura, M.; Akamatsu, K.; Deki, S. Synthesis of Titanium Carbide from a Composite of TiO_2 Nanoparticles/Methyl Cellulose by Carbothermal Reduction. *Mater. Res. Bull.* **2001**, *36*, 2263–2275.
4. Huber, P.; Manova, D.; Mandl, S.; Rauschenbach, B. Formation of TiN, TiC, and TiCN by Metal Plasma Immersion Ion Implantation and Deposition. *Surf. Coat. Technol.* **2003**, 174–175, 1243−1247.
5. Tong, L. R.; Reddy, R. G. Synthesis of Titanium Carbide Nanopowder by Thermal Plasma. *Scrip. Mater.* **2005**, *52*, 1253–1258.
6. Tjong, S. C.; Ma, Z. Y. Microstructural and Mechanical Characteristics of *in Situ* Metal Matrix Composites. *Mater. Sci. Eng. R* **2000**, *29*, 49–113.
7. Oyama, S. T. Preparation and Catalytic Properties of Transition-Metal Carbides and Nitrides. *Catal. Today* **1992**, *15*, 179–200.
8. Chen, J. G. and Nitride Overlayers on Early Transition Metal Surfaces: Preparation, Characterization, and Reactivities. *Chem. Rev.* **1996**, *96*, 1477–1498.
9. Calais, J.-L. Band-Structure of Transition-Metal Compounds. *Adv. Phys.* **1977**, *26*, 847–885.
10. Neckel, A. Recent Investigations on the Electronic-Structure of the 4th-Group and 5th-Group Transition-Metal Monocarbides, Mononitrides, and Monoxides. *Int. J. Quantum Chem.* **1983**, *23*, 1317–1353.
11. Schwartz, K. Band Structure and Chemical Bonding in Transition Metal Carbides and Nitrides. *CRC Crit. Rev. Solid State Mater. Sci.* **1987**, *13*, 211–257.
12. Haruta, M. Size- and Support-Dependency in the Catalysis of Gold. *Catal. Today* **1997**, *36*, 153–166.
13. Valden, M.; Lai, X.; Goodman, D. W. Onset of Catalytic Activity of Gold Clusters on Titania with the Appearance of Nonmetallic Properties. *Science* **1998**, *281*, 1647–1650.
14. Campbell, C. T.; Parker, S. C.; Starr, D. E. The Effect of Size-Dependent Nanoparticle Energetics on Catalyst Sintering. *Science* **2002**, *298*, 811–814.
15. Hwu, H. H.; Chen, J. G. Surface Chemistry of Transition Metal Carbides. *Chem. Rev.* **2005**, *105*, 185–212.
16. Levy, R. B.; Boudart, M. Platinum-like Behavior of Tungsten Carbide in Surface Catalysis. *Science* **1973**, *181*, 547–549.
17. Oyama S. T. *The Chemistry of Transition Metal Carbides and Nitrides;* Chapman & Hall: New York, 1996; p 439−454.
18. Iglesia, E.; Ribeiro, F. H.; Boudart, M.; Baumgartner, J. E. Synthesis, Characterization, and Catalytic Properties of Clean and Oxygen-Modified Tungsten Carbides. *Catal. Today* **1992**, *15*, 307–337.
19. Narayanan, R.; El-Sayed, M. A. Raman Studies on the Reactants with the Platinum Nanoparticle Surface during

the Nanocatalyzed Electron Transfer Reaction. *J. Phys. Chem. B* **2005**, *109*, 18460–18464.
20. Zecchina, A.; Groppo, E.; Bordiga, S. Selective Catalysis and Nanoscience: An Inseperable Pair. *Chem.—Eur. J.* **2007**, *13*, 2440–2460.
21. Oshima, C.; Aono, M.; Otani, S.; Ishizawa, Y. The Hydrogen Chemisorption on TiC(111) Surface Studied by High-Resolution Electron-Energy Loss Spectroscopy. *Solid State Commun.* **1983**, *18*, 911–913.
22. Merrill, P. B.; Perry, S. S.; Frantz, P.; Didziulis, S. V. Adsorption of Water on TiC(100): Evidence for Complex Reaction and Desorption Pathways. *J. Phys. Chem. B* **1998**, *102*, 7606–7612.
23. Didziulis, S. V.; Frantz, P.; Perry, S. S.; El-bjeirami, O.; Imaduddin, S.; Merrill, P. B. Substrate-Dependent Reactivity of Water on Metal Carbide Surfaces. *J. Phys. Chem. B* **1999**, *103*, 11129–11140.
24. Frantz, P.; Didziulis, S. V.; Fernandez-Torres, L. C.; Guenard, R. L.; Perry, S. S. Reaction of Methanol with TiC and VC (100) Surfaces. *J. Phys. Chem. B* **2002**, *106*, 6456–6464.
25. Guenard, R. L.; Fernandez-Torres, L. C.; Kim, B.-I.; Perry, S. S.; Didziulis, S. V.; Frantz, P. The Interaction of Ammonia with Transition Metal Carbide Surfaces. *Surf. Sci.* **2002**, *511*, 121–132.
26. Fernandez-Torres, L. C.; Perry, S. S.; Guenard, R. L.; Kim, B.-I.; Frantz, P.; Didziulis, S. V. Selective Surface Reactions of Single Crystal Metal Carbides: Alkene Production from Short Chain Alcohols on Titanium Carbide and Vanadium Carbide. *Surf. Sci.* **2002**, *515*, 103–116.
27. Didziulis, S. V.; Frantz, P.; Fernandez-Torres, L. C.; Guenard, R. L.; El-bjeirami, O.; Perry, S. S. Coordination Chemistry of Transition Metal Carbide Surfaces: Detailed Spectroscopic and Theoretical Investigations of CO Adsorption on TiC and VC (100) Surfaces. *Phys. Chem. B* **2001**, *105*, 5196–5209.
28. Frantz, P.; Kim, H. I.; Didziulis, S. V.; Li, S.; Chen, Z.; Perry, S. S. Reaction of Methyl Formate with VC(100) and TiC(100) Surface. *Surf. Sci.* **2005**, *596*, 144–162.
29. Vines, F.; Sousa, C.; Illas, F.; Liu, P.; Rodriguez, J. A. A Systematic Density Functional Study of Molecular Oxygen Adsorption and Dissociation on the (001) Surface of Group IV−VI Transition Metal Carbides. *J. Phys. Chem. C* **2007**, *111*, 16982–16989.
30. Vines, F.; Sousa, C.; Illas, F.; Liu, P.; Rodriguez, J. A. Density Function Study of the Adsorption of Atomic Oxygen on the (001) Surface of Early Transition-Metal Carbides. *J. Phys. Chem. C* **2007**, *111*, 1307–1314.
31. Rodriguez, J. A.; Liu, P.; Dvorak, J.; Jirsak, T.; Gomes, J.; Takahashi, Y.; Nakamura, K. Adsorption and Decomposition of SO_2 on TiC(001): An Experimental and Theoretical Study. *Surf. Sci.* **2003**, *543*, L675–L682.
32. Rodriguez, J. A.; Liu, P.; Dvorak, J.; Jirsak, T.; Gomes, J.; Takahashi, Y.; Nakamura, K. The Interaction of Oxygen with TiC(001): Photoemission and First-Principle Studies. *J. Chem. Phys.* **2004**, *121*, 465–474.
33. Harbuck, D. D.; Davidson, C. F.; Monte, B. Gas-Phase Production of Titanium Nitride and Carbide Powders. *J. Metals* **1986**, *38*, 47–50.
34. Xiang, D.; Liu, Y.; Zhao, Z.; Cao, H.; Gao, S.; Tu, M. Reaction Sequence and Influence Factors during Preparation of Ti(C, N) Powders. *J. Alloys Compd.* **2007**, *429*, 264–269.
35. Tomita, S.; Andrzej, B.; Dore, J. C.; LeBolloch, D.; Fujii, M.; Shinji, H. Diamond Nanoparticle to Carbon Onions Transformation: X-ray Diffraction Studies. *Carbon* **2002**, *40*, 1469–1474.
36. Rodriguez, P.; Munoz-Aguirre, N.; San-Martin Martinez, E.; Gonzalez, G.; Zelaya, O.; Mendoza, J. Formation of CdS Nanoparticles using Starch as Capping Agent. *Appl. Surf. Sci.* **2008**, *255*, 740–742.
37. Cullity B. D. *Elements of X-ray Diffraction,* 2nd ed.: Addison-Wesley: Reading, MA, 1978; p 115.
38. Suryananarayana, C.; Grant Norton, M. *X-ray Diffraction: A Practical Approach;* Plenum: New York, 1998; p 97.
39. Xia, Y.; Xiong, Y.; Lim, B.; Skrabalak, S. E. Shape-Controlled Synthesis of Metal Nanocrystals: Simple Chemistry Meets Complex Physics. *Angew. Chem., Int. Ed.* **2009**, *48*, 60–103.
40. Wulff, G. On the Question of Speed of Growth and Dissolution of Crystal Surfaces. *Z. Kristallogr.* **1901**, *34*, 449–530.
41. Sunagawa, I. *Morphology of Crystals, Part A*; Terra Scientific: Boston, MA, 1987; p 271−319.
42. Lee, B.; Komarneni, S. *Chemical Processing of Ceramics*; Taylor & Francis: New York, 2005; p 517−522.
43. Radenovic, N.; Enckevort, W.; Vlieg, E. Formamide Adsorption and Habit Changes of Alkali Halide Crystal Grown from Solutions. *J. Cryst. Growth* **2004**, *263*, 544–551.
44. Millstone, J. E.; Wei, W.; Jones, M. R.; Yoo, H.; Mirkin, C. A. Iodide Ions Control Seed-Mediated Growth of Anisotropic Gold Nanoparticles. *Nano Lett.* **2008**, *8*, 2526–2529.